PHYSICAL REVIEW E **71**, 045601(R) (2005)

Spatial and temporal turbulent velocity and vorticity power spectra from sound scattering

Shahar Seifer[1] and Victor Steinberg[1,2]
[1]*Department of Physics of Complex Systems, Weizmann Institute of Science, Rehovot 76100, Israel*
[2]*International Center for Theoretical Physics, Strada Costiera 11, I-34100 Trieste, Italy*
(Received 17 August 2004; revised manuscript received 26 October 2004; published 13 April 2005)

By performing sound-scattering measurements with a detector array consisting of 62 elements in a flow between two counter-rotating disks we obtain the energy and vorticity power spectra directly in both spatial and temporal domains. Fast-accumulated statistics and a large signal-to-noise ratio allow us to get high-quality data rather effectively and to test scaling laws in details.

DOI: 10.1103/PhysRevE.71.045601 PACS number(s): 47.32.−y, 43.30+m, 43.35+d

One of the challenging experimental tasks in studies of turbulent flows is developing new tools to characterize velocity and vorticity fields in spatial and temporal domains. Ultrasound scattering by flow is regarded as a promising approach in this respect. First, sound is the only remotely accessible nonperturbing probe of flow that does not require seeding particles. Second, at rather widely satisfied conditions, a direct relation between the scattering signal and the spatial Fourier transform of either velocity or vorticity fields exists. Spatial characterization of velocity that is not based on the Taylor's frozen flow assumption is one of the goals of experimental turbulence. Particle image velocimetry (PIV) is capable of performing this task but it requires seeding particles and extensive data transferring from a camera. The main advantage of the sound scattering compared with PIV particularly shows up in studies of fast dynamics in a flow.

There were a few studies in the past to experimentally probe turbulent flow by the sound-scattering method. These experiments were based on a single moving transducer arrangement and concentrated on studies of angular distribution of scattered waves in atmospheric turbulence [1] and in grid turbulence in a wind tunnel [2]. However, the quality of the data permitted just to test consistency of the relation between scattering cross section and turbulent energy spectrum [8]. Later the vorticity distribution [3] in a swirling jet as well as the temporal dynamics of vorticity fluctuations [4,5] and a large scale circulation in high Reynolds numbers flows [6,7] were also investigated.

In this Rapid Communication we present results of the simultaneous acquisition of 62 acoustic detectors arranged on the cell wall in front of a linear emitter in the same plane [7]. The far-field scattering values required by the theory [8–10] are acquired owing to a wave-construction method similar to the Huygens principle in optics. The limitation due to either a finite sound beam width or an aperture discussed in Ref. [7] is released since (i) they are of the order of the integral scale of velocity fluctuations, and (ii) the edge diffraction of the scattering wave cancels out with time due to the randomness of the flow. Thus, the amplitude of the complex wave function of the scattering sound in the far-field limit can be related to the two-dimensional (2D) spatial Fourier transform of the velocity field (and also the vorticity) as follows [9,10]:

$$\frac{\Psi_{scat}}{\Psi_{rest}}(\vec{r},t)=\frac{1}{c}\frac{(2\pi k_0)^2\exp(i\pi/4)}{\sqrt{2\pi k_0 r}}\cos\theta F_{\vec{k_s}}\{v_x\}, \qquad (1)$$

where $\Psi_{scat}=\Psi-\Psi_{rest}$, and Ψ and Ψ_{rest} are the complex wave functions that describe the sound pressure oscillations in the presence of a flow and without it, respectively; k_0 and c are the sound wave number and the velocity, respectively; θ and k_s are the scattering angle and the wave number, respectively, that are related to each other via $k_s\equiv|\vec{k_s}|=2k_0\sin\theta/2$; and $r=|\vec{r}|$ is the distance from the center of a scattering region till a detector. $F_{\vec{k_s}}\{v_x\}$ is the 2D Fourier transform of the velocity component in the forward direction of the beam that is related to the Fourier transform of the vorticity via $F_{\vec{k_s}}\{v_x\}=(i/2k_0)\cot(\theta/2)F_{\vec{k_s}}\{(\vec{\nabla}\times\vec{v})_z\}$.

The construction of the far-field scattering wave function from the near-field measurements is based on a mathematical description of the Huygens principle and derived from the Rayleigh-Sommerfeld integral [11] as

$$\Psi(r_f,y)^{ff}_{scat}=\int\frac{k_0 i^{3/2}dy'}{\sqrt{2\pi k_0(r_f-r_d)}}e^{i[k_0(y-y')^2]/[2(r_f-r_d)]}\Psi(r_d,y')^{d}_{scat}, \qquad (2)$$

where r_d and r_f are the distances measured from the cell center till the detector and the far-field region, respectively; $\Psi(0,y')^{d}_{scat}$ and $\Psi(x,y)^{ff}_{scat}$ are the scattering wave functions at the detector (as measured) and at the far-field, respectively [7].

Measuring scattering around the forward direction with high-frequency sound guarantees avoiding interference from the scattering of sound beam side lobes. Either a finite flow extent or a finite beamwidth eliminate any scattering amplitude divergence in the forward direction [12]. In general, the scattering field of ultrasound in the small Mach number approximation is the result of phase shifts induced by entrainment of the wave by the flow, and additional effects are the influence from the spatial derivative of velocity in the beam direction and the influence of diffraction of those distortions. The latter effect is the reason that simple analysis of the phase shifts is not sufficiently accurate.

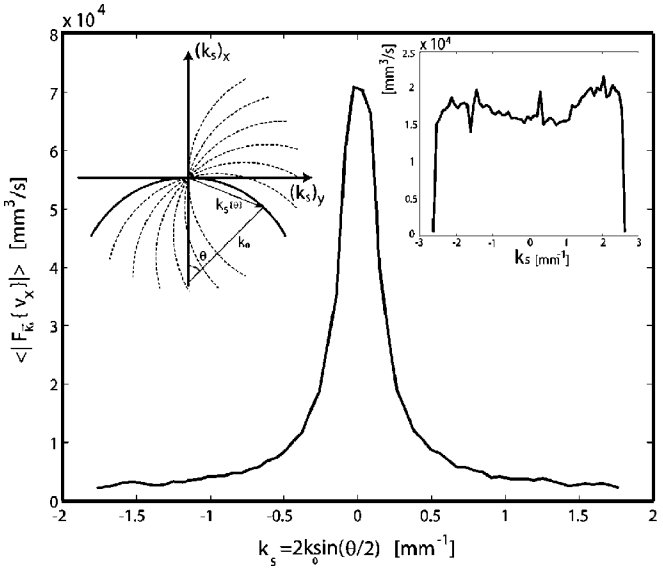

FIG. 1. Time-averaged velocity structure function obtained by sound scattering via the far-field construction taken at $\mathrm{Re}=1.5\times10^6$ and 3 MHz. Right inset: The same property obtained from sound-scattering data at the detector without far-field construction. Left inset: The path in the wave number plane (solid line), on which information on the velocity (vorticity) spectrum for a given beam direction is obtained; other curves (dashed lines) contain information on scattering from sound beams emitted in various directions.

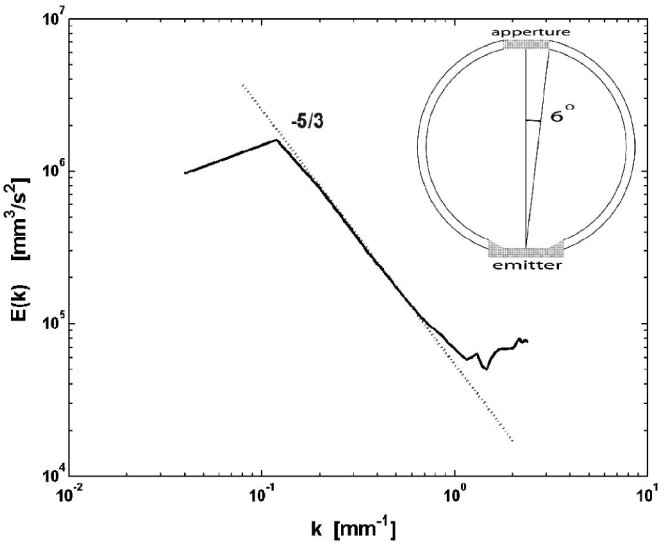

FIG. 2. Energy spectrum derived from the data presented in Fig. 1. Inset: The scheme of the aperture limit for the sound detector array.

The experimental setup is described in detail in Ref. [7]. The von Karman swirling water flow was produced between two counter-rotating disks of a diameter $2R=280$ mm with four triangular blades of 20-mm high and 5-mm thick and with rims. They are driven by two dc brushless motors, whose velocity is controlled with a stability of about 0.1% via optical encoders. This setup is well recognized to generate a strong intensity turbulent flow in a confined region (see, for example [4]). The flow is confined by a perspex cylinder with an inner diameter 290 mm and 320 mm in height and disks separation of 205 mm. By changing a rotation frequency, the Reynolds number, $\mathrm{Re}=2\Omega R^2/\nu$, is varied between 2.5×10^5 and 1.7×10^6 that corresponds to the Taylor microscale Reynolds number R_λ between 200 and 570. Here Ω is the angular velocity of the disk, ν is the kinematic viscosity, and the energy dissipation, $\epsilon=4.9\times10^{-18}\mathrm{Re}^3$ W/kg, and the rms of the velocity fluctuations in the middle plane, $V_{rms}=0.5\times10^{-6}\mathrm{Re}$ m/sec, obtained from the global torque and the hot wire anemometry (HWA) measurements, respectively [13].

The sound-scattering measurements were conducted in the middle plane between the disks and in the plane at 30 mm below it. The emitter was 80 mm long and 10 mm wide, and the size of the scattering region was defined by the length of the detector designed as a linear array of 62 acoustic detectors with 1-mm spacing and 62×10 mm^2 active area (from Blatek). Thus, the velocity is averaged across the beam thickness of 10 mm that is quite larger than the Taylor scale. A range of frequencies covered in the experiment was between 1 and 7 MHz. The acquisition system is built in a heterodyne scheme that is based on 62 lock-in amplifiers with 62 preamplifiers. The details of the design and its operation are presented in Ref. [7]. Every sound pulse is sampled exactly simultaneously by 62 lock-in detectors combined with sample and hold components, so 0° and 90° products (fluctuation values of the complex wave function) are recorded. A typical sound propagation time through the cell is about 200 μs that is a typical freezing time segment. Within this period one pulse is sent, and the flow is almost frozen. In such way the instantaneous fluctuations in sound due to scattering by the flow can be used to characterize the velocity components in the plane in which the beam propagates to the detector array.

Scattering from a single incident beam provides information about the velocity (vorticity) field only on a single curve in a $((k_s)_x,(k_s)_y)$ plane (see Fig. 1, left inset, solid line). To get information on other curves in the plane (see Fig. 1, left inset, dashed lines) requires us to use sound beams emitted by different transducers in many different directions simultaneously. Then complete structure functions of the velocity (vorticity) fluctuations can be retrieved without any assumption about isotropy and homogeneity of a turbulent flow. However, with only one emitter at hand and the detector array we should rely on the isotropy and homogeneity assumptions of the turbulent flow under studies. Thus in the present case the sound scattering provides direct measurements of the energy spectrum as well as the Fourier transform of the vorticity structure function in a spatial domain that are related as $E(k_s)=6\pi^3/Ak_s|F_{\vec{k}_s}\{(\vec{\nabla}\times\vec{v})_z\}|^2$. Here the kinetic energy per unit mass is defined as $\int E(k)dk=(3/2A)\int v_x^2 d^2r$, where A is the cross-sectional area of a sound beam. In Fig. 1 we present a typical result on the time-averaged velocity Fourier transform in the far field obtained from the scattering wave function via Eq. (1) and the far-field reconstruction according to Eq. (2). The same function, but observed directly in the detector plane, looks drastically different (see right inset in Fig. 1). These data are the result of averaging on 60 000 sound pulses at a 1.8-kHz rep-

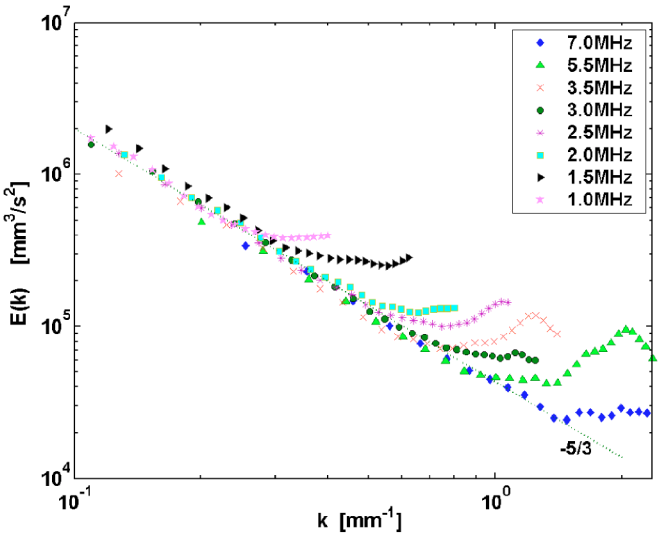

FIG. 3. (Color online) Energy spectra taken at various sound frequencies from 1 up to 7 MHz at $\mathrm{Re}=1.2\times10^6$.

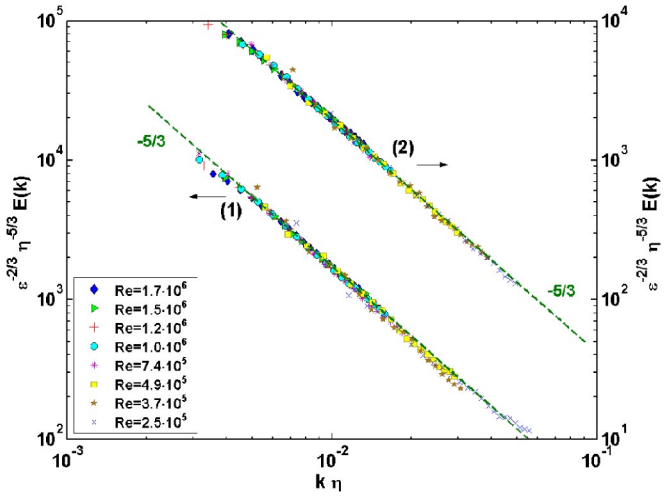

FIG. 4. (Color online) Scaled energy spectra as a function of the reduced wave number at various Re: (1) at $h=0$, (2) at $h=-30$ mm. The dashed lines show the Kolmogorov scaling law with the exponent $-5/3$.

etition rate and at a frequency of 3 MHz taken in the von Karman swirling flow at $\mathrm{Re}=1.5\times10^6$.

In Fig. 2 the resulting energy spectrum as a function of the wave number is shown. The dotted line denotes the "$-5/3$" slope according to the Kolmogorov law to demonstrate that indeed in some range of the wave numbers the spectrum follows the expected law. It can be compared with the results on the energy spectra obtained by PIV, where, though, a shorter scaling region is also observed [13]. In the sound measurements shown in Fig. 2 the wave numbers are limited by the range of values $0.1<k<0.8$ mm^{-1}, outside of which the spectrum cannot be retrieved. The lower side of the range of k is limited by the beamwidth, i.e., one cannot get information on a scale exceeding the beamwidth (in the energy spectra from PIV the scaling region begins already at $k=0.06$ mm^{-1} for $\mathrm{Re}>10^6$). On the higher side of the range, the ultimate limit is determined by the size of the element in the detector array, namely, $k_{max}\leqslant 2\pi$ mm^{-1} corresponding to a 1-mm detector array spacing. However, even before this limit is reached, the energy spectrum is cut on the higher wave number side by the visibility at large scattering angles through the detector aperture. It means that some sound rays are blocked by the limited length of the detector array. According to the detector array length and the cell diameter at angles exceeding about 6°, the visibility starts to deteriorate (see the inset in Fig. 2). The corresponding limit is $k_{s_{(lim)}}=2k_0\sin(\theta_{max}/2)\simeq 0.1k_0$. It gives about 1.3 mm^{-1} at 3 MHz compared to 0.8 mm^{-1} observed. We tested this relation at various frequencies, and the results on the energy spectra taken at different sound frequencies are presented in Fig. 3. One finds that by changing the frequency from 1 up to 7 MHz the upper wave number limit moves linearly toward the highest value of about 1.5 mm^{-1}, but still far away from $k_{max}=2\pi$ mm^{-1}.

Useful information in terms of the turbulent flow energy dissipation, ϵ, can be gained from the combined presentation of the energy spectra obtained from the sound-scattering measurements at different Reynolds numbers. There is a known scaling law for the energy spectra [14–16] that appears as the result of plotting the scaled energy density spectrum $\epsilon^{-2/3}\eta^{-5/3}E(k)$ vs $k\eta$, where η is the Kolmogorov dissipation scale defined as $\eta=(\nu^3/\epsilon)^{1/4}$ [16]. The idea is to find the best match between the scaled spectra at different Re with fitting values of ϵ. It turns out that the scaling exists for the data at all values of Re, and the results for the sound scattering in the middle plane (curve 1) and in the plane at 30 mm below it (curve 2) are shown in Fig. 4. Each data set for each Re consists of 4×10^6 points. The dependence of the energy dissipation, ϵ, on Re is found to be $\epsilon\sim\mathrm{Re}^{3.1\pm0.1}$ with a good quality of the fits. The exponent value is rather close to 3, the expected one according to the dimensional analysis [13,17] (compare with the expression for ϵ presented above).

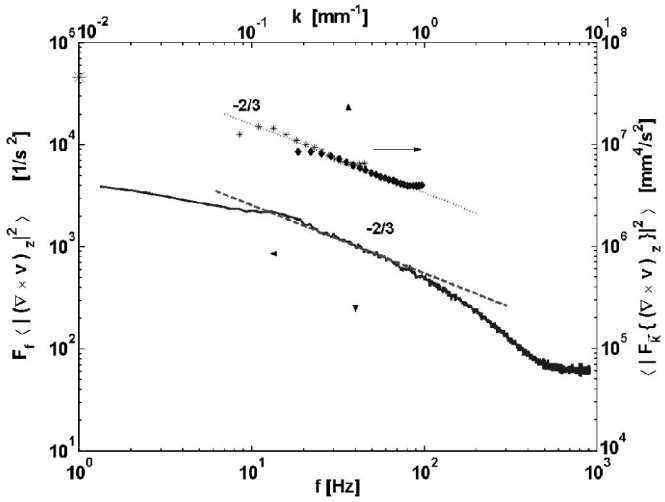

FIG. 5. Upper curve: Power spectra of the time-averaged vorticity as a function of k taken at $\mathrm{Re}=1.2\times10^6$ and frequencies 2.5 (asterisks) and 5.8 (diamonds) MHz. Lower curve: Power spectra of space-averaged enstrophy as a function of f. The dashed lines show the Kolmogorov scaling with the exponent $-2/3$.

The Kolmogorov constant C in the Kolmogorov equation $\epsilon^{-2/3}\eta^{-5/3}E(k)=C(k\eta)^{-5/3}$ is determined experimentally from the fit of the plots in Fig. 4, and the value is $C\simeq 0.8$ for the curve (1) and $C\simeq 0.9$ for the curve (2).

We also calculate the integral scale in the flow at Re $=1.2\times 10^6$, using [18] $L_{int}=(3\pi/4)\int k^{-1}E(k)dk/\int E(k)dk$ $=40\pm 10$ mm, based on the system scale 0.02 mm^{-1} and the scaling region $0.06<k<1.5$ mm^{-1}. This value occurs to be rather close to the beamwidth, and the corresponding wave number is located close to the lower end of the wave number range of the spectrum.

To test the Taylor hypothesis [16,18] for the swirling flow the energy spectrum in the frequency domain is calculated as $E(f)=1/T\int_0^T E(t)\exp(-i2\pi ft)dt$ and $E(t)=\int 6\pi^3/Ak_s|F_{\vec{k}_s}(\vec{\nabla}\times\vec{v}(t))_z|^2d^2k_s$. A proper energy spectrum can be obtained only if the lowest k_s is available due to the pole at k_s^{-1} in the integrand. So we turn out to the Fourier transform of the vertical vorticity. In Fig. 5 (upper curve) we present the time-averaged power spectrum of the vorticity as a function of k (based on 2×10^7 points) at Re$=1.2\times 10^6$ obtained at the sound frequencies 2.5 MHz (asterisks) and 5.8 MHz (diamonds). The dashed line with the scaling exponent $-2/3$ represents the expected dependence according to the Kolmogorov predictions [16,18]. It can be compared with the space-averaged over the beam area Fourier transform of the enstrophy in the frequency domain $N(f)$ $=1/T\int_0^T N(t)\exp(-i2\pi ft)dt$, where $N(t)=1/A\int_A|(\vec{\nabla}\times\vec{v}(t))_z|^2d^2r=(2\pi)^2\int|F_{\vec{k}_s}(\vec{\nabla}\times\vec{v}(t))|^2d^2k_s$. The latter shows a rather wide scaling region (see the lower curve in Fig. 5). The advection velocity, V_T, found from the two plots in Fig. 5 is $V_T=2\pi f/k\simeq 0.6$ m/s that is rather close to the average velocity [13].

We would like to point out also that the mean enstrophy value, marked in Fig. 5 by asterisk on the left-hand side ordinate axis, is about an order of magnitude larger than one corresponding to a rigid body rotation with the same rotation velocity of 300 rpm and the vorticity of 63 s^{-1}, or the enstrophy of about 4000 s^{-2}. In the corotational disks geometry at the same parameters and with a large scale single vortex flow configuration the enstrophy is also much lower [7].

This work was partially supported by an Israel Science Foundation grant, by a Binational U.S.-Israel Foundation grant, and by the Minerva Center for Nonlinear Physics of Complex Systems.

[1] M. A. Kallistratova, Sov. Phys. Acoust. **5**, 512 (1959).
[2] W. Baerg and W. H. Schwartz, J. Acoust. Soc. Am. **39**, 1125 (1966).
[3] M. Oljaca, X. Gu, A. Glezer, M. Baffico, and F. Lund, Phys. Fluids **10**, 886 (1998).
[4] B. Dernoncourt, J.-F. Pinton, and S. Fauve, Physica D **117**, 181 (1998).
[5] C. Baudet, O. Michel, and W. J. Williams, Physica D **128**, 1 (1999).
[6] R. Berthet, S. Fauve, and R. Labbe, Eur. Phys. J. B **32**, 237 (2003).
[7] Sh. Seifer and V. Steinberg, Phys. Fluids **16**, 1587 (2004).
[8] R. H. Kraichnan, J. Acoust. Soc. Am. **25**, 1096 (1953).
[9] A. L. Fabricant, Sov. Phys. Acoust. **29**, 152 (1983).
[10] F. Lund and C. Rojas, Physica D **37**, 508 (1989).
[11] P. L. Marston, in *Physical Acoustics*, edited by A. Pierce and R. Thurston (Academic, London, 1992), Vol. XXI.
[12] R. Bertet and F. Lund, Phys. Fluids **7**, 2522 (1995).
[13] Sh. Seifer, Ph.D. thesis, Weizmann Institute of Science, Rehovot, 2004 (unpublished); and Sh. Seifer and V. Steinberg (unpublished).
[14] M. Nelkin, Science **255**, 566 (1992).
[15] S. G. Saddoughi and S. V. Veeravalli, J. Fluid Mech. **268**, 333 (1994).
[16] U. Frisch, *Turbulence: The Legacy of A.N. Kolmogorov* (Cambridge University Press, Cambridge, 1995).
[17] O. Cadot, Y. Couder, A. Daerr, S. Douady, and A. Tsinober, Phys. Rev. E **56**, 427 (1997).
[18] M. Lesieur, *Turbulence in Fluids* (Kluwer Academic, Dordrecht, 1997).